A Modular PIP_2 Binding Site as a Determinant of Capsaicin Receptor Sensitivity

Elizabeth D. Prescott and David Julius

Science **300**, 1284 (2003);
DOI: 10.1126/science.1083646

Science (print ISSN 0036-8075; online ISSN 1095-9203) is published weekly, except the last week in December, by the American Association for the Advancement of Science, 1200 New York Avenue NW, Washington, DC 20005.

D. B. Shaw, Ed., (Royal Meteorological Society of London, London, 1979), pp. 251–259.
25. B. D. Santer *et al.*, *J. Geophys. Res.* **100**, 10693 (1995).
26. E. Roeckner, L. Bengtsson, J. Feichter, J. Lelieveld, H. Rodhe, *J. Clim.* **12**, 3004 (1999).
27. M. R. Allen, S. F. B. Tett, *Clim. Dyn.* **15**, 419 (1999).
28. P. A. Stott *et al.*, *Science* **290**, 2133 (2000).
29. G. C. Hegerl *et al.*, *J. Clim.* **9**, 2281 (1996).
30. P. A. Stott, S. F. B. Tett, *J. Clim.* **11**, 3282 (1998).
31. S. F. B. Tett *et al.*, *J. Geophys. Res.* **107**, doi 10.1029/2000JD000028 (2002).
32. V. Ramaswamy *et al.*, in *Climate Change 2001: The Scientific Basis*, J. T. Houghton *et al.*, Eds. (Cambridge Univ. Press, Cambridge, 2001), pp. 349–416.
33. The PCM climate change experiments available to us did not consider indirect aerosol forcing. However, we did have access to an ECHAM experiment that incorporated the indirect effects of anthropogenic sulfate aerosols on cloud albedo (*26*). Like the PCM ALL experiment, the ECHAM integration (GSDIO) applied changes in well-mixed greenhouse gases, sulfate aerosol direct effects, and tropospheric ozone. GSDIO differed from ALL both in its inclusion of indirect sulfate aerosol effects and in its neglect of changes in solar irradiance, volcanic aerosols, and stratospheric ozone. These differences in the ALL and GSDIO forcings (and the fact that no ECHAM experiment included all GSDIO forcings except indirect sulfate aerosols) make it difficult to isolate the influence of indirect sulfate aerosols on the detection of T4 and T2 fingerprints. Nevertheless, we note that repeating our detection analysis with GSDIO fingerprints yields results qualitatively similar to those obtained with PCM (fig. S2 and Fig. 4, respectively). This suggests that our primary conclusions may be relatively insensitive to the inclusion of indirect sulfate aerosol effects. The main difference between the PCM and ECHAM results is the delayed and less robust detection of the GSDIO mean-removed T4 fingerprint, which is probably due to GSDIO's neglect of stratospheric ozone depletion. Another difference is that the GSDIO mean-removed T2 fingerprint is detected earlier and more consistently than the corresponding PCM ALL fingerprint.
34. J. R. Lanzante, S. A. Klein, D. J. Seidel, *J. Clim.* **16**, 241 (2003).
35. F. J. Wentz, M. Schabel, *Nature* **403**, 414 (2000).
36. J. F. B. Mitchell *et al.*, in *Climate Change 2001: The Scientific Basis*, J. T. Houghton *et al.*, Eds. (Cambridge Univ. Press, Cambridge, 2001), pp. 695–738.
37. Work at Lawrence Livermore National Laboratory (LLNL) was performed under the auspices of the U.S. Department of Energy (DOE), Environmental Sciences Division, contract W-7405-ENG-48. T.M.L.W. was supported by the National Oceanic and Atmospheric Administration Office of Global Programs ("Climate Change Data and Detection") grant no. NA87GP0105, and by DOE grant no. DE-FG02-98ER62601. A portion of this study was supported by the DOE Office of Biological and Environmental Research, as part of its Climate Change Prediction Program. The MSU T2 and T4 data and static MSU weighting functions were provided by J. Christy (Univ. of Alabama in Huntsville). ECHAM model data were supplied by E. Roeckner. We thank T. Barnett and an anonymous reviewer for useful comments and suggestions.

Supporting Online Material
www.sciencemag.org/cgi/content/full/1082393/DC1
SOM Text
Figs. S1 and S2

15 January 2003; accepted 23 April 2003
Published online 1 May 2003;
10.1126/science.1082393
Include this information when citing this paper.

A Modular PIP_2 Binding Site as a Determinant of Capsaicin Receptor Sensitivity

Elizabeth D. Prescott and David Julius*

The capsaicin receptor (TRPV1), a heat-activated ion channel of the pain pathway, is sensitized by phosphatidylinositol-4,5-bisphosphate (PIP_2) hydrolysis after phospholipase C activation. We identify a site within the C-terminal domain of TRPV1 that is required for PIP_2-mediated inhibition of channel gating. Mutations that weaken PIP_2-TRPV1 interaction reduce thresholds for chemical or thermal stimuli, whereas TRPV1 channels in which this region is replaced with a lipid-binding domain from PIP_2-activated potassium channels remain inhibited by PIP_2. The PIP_2-interaction domain therefore serves as a critical determinant of thermal threshold and dynamic sensitivity range, tuning TRPV1, and thus the sensory neuron, to appropriately detect heat under normal or pathophysiological conditions.

Charged membrane phospholipids are thought to regulate a variety of ion channels and transporters (*1*). For example, recent electrophysiological studies suggest a role for the membrane phospholipid PIP_2 as a modulator of transient receptor potential (TRP) channels, many of which contribute to the detection of sensory stimuli. TRP channels in the *Drosophila* eye (*2*) and TRPV1 channels in the mammalian pain pathway (*3*, *4*) are activated or potentiated when PIP_2 is hydrolyzed, whereas the ubiquitously expressed mammalian TRPM7 channel is inhibited by PIP_2 cleavage (*5*). Phospholipase C (PLC) catalyzes the hydrolysis of PIP_2 to inositol trisphosphate (IP_3) and diacylglycerol (DAG) and has been implicated in the release of TRPV1 from PIP_2-mediated inhibition (*3*), although the underlying mechanism for such regulation has not been elucidated. Despite functional evidence that TRP channels are directly regulated by PIP_2, there is now no structural basis to account for this effect. TRPV1 is an especially tractable model for addressing this question, because it can be directly gated by a number of stimuli, including the pungent vanilloid compound capsaicin, extracellular protons (pH $<$ 6.0), or noxious heat ($>$43°C) (*6*, *7*). Moreover, genetic studies have shown that TRPV1 is an essential component of the signaling pathway through which PLC-coupled receptors increase behavioral sensitivity to heat (*3*, *8*, *9*), which makes elucidation of this regulatory pathway of physiological interest.

To investigate the molecular basis of PIP_2-dependent regulation, we determined which regions of TRPV1 were required for PLC-mediated potentiation. We reasoned that mutations affecting such domains should render TRPV1 insensitive to PIP_2 inhibition, and therefore, we identified mutants exhibiting increased responses to capsaicin or extracellular protons. A TRPV1 mutant lacking a segment of the C-terminal cytoplasmic domain (TRPV1 Δ777–820) produced much larger currents than wild-type channels in response to low doses of capsaicin (250 nM) or protons (pH 5.5), when expressed in *Xenopus* oocytes (Fig. 1). These enhanced currents could not be attributed to increased cell surface expression, because biotinylation experiments revealed equivalent levels of the mutant and wild-type TRPV1 at the plasma membrane (fig. S1). To determine whether amino acids 777 to 820 were also required for PLC-mediated potentiation, we exposed oocytes expressing TRPV1 channels and the nerve growth factor (NGF) receptor TrkA/p75 to NGF, a treatment that normally elicits a robust potentiation wild-type TRPV (~20-fold) of responses through activation of PLC-γ (*3*). Currents from TRPV1Δ777–820 were unchanged, which suggests that these residues are critical for mediating potentiation downstream of PLC-coupled receptor stimulation. Moreover, potentiation of TRPV1Δ777–820 was not observed when other PLC-coupled receptors were activated, including the epidermal growth factor receptor (EGFR) and the G protein–coupled m1 muscarinic acetylcholine receptor (*10*). Loss of potentiation was not simply due to increased agonist sensitivity of the mutant channel, because the response to either a low dose of capsaicin (100 nM) or protons (pH 6.1) was unchanged after PLC activation (*10*). In addition, the thermal threshold of TRPV1Δ777–820 was markedly shifted to lower temperatures, and the overall currents were larger than those of wild-type channels (Fig. 1D), a phenotype reminiscent of wild-type channels that have been potentiated by PLC-coupled receptor activation (*3*).

Department of Cellular and Molecular Pharmacology, University of California, San Francisco, CA 94143–2140, USA.

*To whom correspondence should be addressed. E-mail: julius@cmp.ucsf.edu

If potentiation of TRPV1 involves release from PIP_2-mediated inhibition, then regions required for potentiation are potential sites of PIP_2 interaction. PIP_2-binding domains of ion channels are loosely characterized by clusters of basic residues interspersed with hydrophobic amino acids, an arrangement that is believed to facilitate interactions with the negatively charged head group of the phospholipid (*1*). In agreement with this, region 777–820 of TRPV1 has a predicted isoelectric point (pI) of 11 and contains eight positively charged residues. To determine which amino acids are most important for mediating potentiation, we generated deletion and point mutations within this region. Removal of as few as 16 residues (777 to 792) completely inhibited potentiation (Fig. 2, A and B). Furthermore, neutralization of as few as two positive charges reduced potentiation by 94 ± 1.1% (Fig. 2B), which suggests that clusters of basic residues are important for mediating TRPV1 potentiation. These mutants not only exhibited increased sensitivity to chemical stimuli, but were also sensitized to heat, as indicated by a shift of activation thresholds to substantially lower temperatures and production of larger currents at suprathreshold temperatures (Fig. 2, C and D). Moreover, as observed for capsaicin- and proton-evoked responses, larger deletions within the 777–820 domain had a more profound phenotype (as indicated by a greater shift in thermal threshold) than small deletions or point mutations, which suggests that residues that affect activation threshold and potentiation are distributed throughout this region.

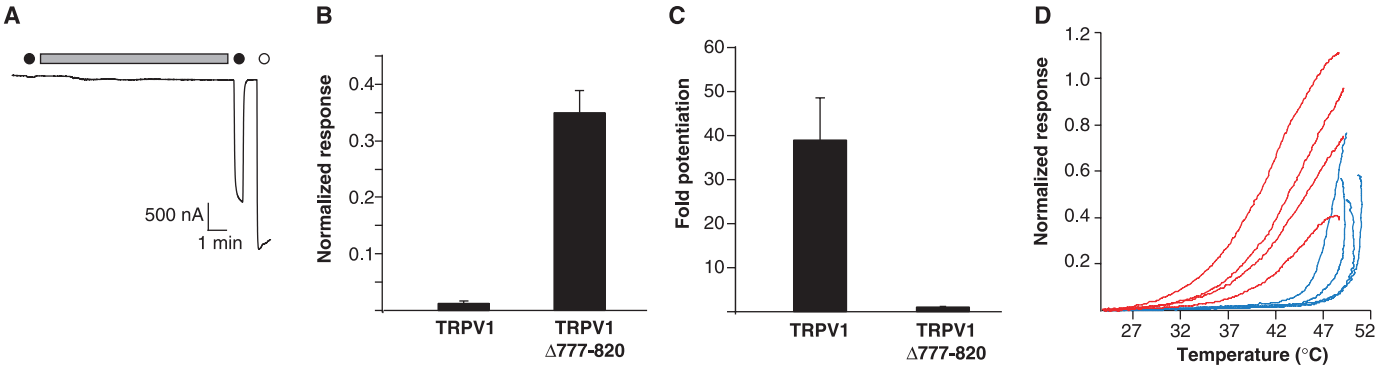

Fig. 1. A C-terminal region of TRPV1 is required for PLC-mediated potentiation. (**A**) Continuous current trace from oocyte expressing TRPV1 and the NGF receptor TrkA/p75 (*24*). Oocyte was exposed to pH 5.5 buffer for 30 s (●), followed by 750 pM NGF for 10 min (gray bar.) After NGF treatment, oocyte was exposed to pH 5.5 again, followed by a saturating (10 μM) dose of capsaicin (○). (**B**) Oocytes expressing indicated channel and TrkA/p75 were challenged with pH 5.5 buffer. Responses were normalized to current evoked with saturating dose of capsaicin (10 μM) according to the protocol indicated in Fig. 1(A). (**C**) Oocytes expressing indicated channels and TrkA/p75 were assayed for PLC-mediated potentiation. Results are measured as the fold increase in response to 30-s challenge with pH 5.5 buffer after 10-min treatment with 750 pM NGF. (**D**) Heat-evoked currents in oocytes expressing TRPV1 (blue traces) or TRPV1Δ777–820 (red traces) were measured in response to temperature ramps and normalized to a saturating dose of capsaicin (10 μM).

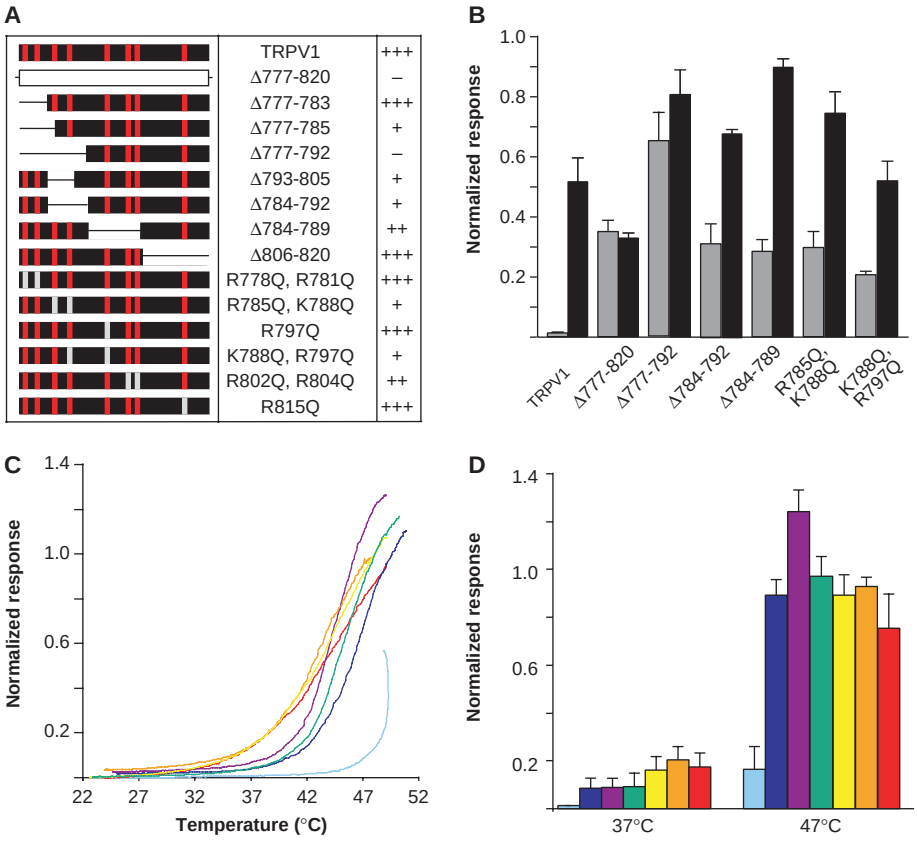

Fig. 2. Delineation of a potentiation domain of TRPV1. (**A**) Representation of amino acid region 777–820 of rat TRPV1. Red boxes indicate basic residues; gray boxes indicate neutralized residues [Lys or Arg replaced by Gln (K→Q or R→Q)]; lines indicate deletions. Relative degree of potentiation obtained with each mutant is indicated at right: (+++) maximal potentiation, (–) no potentiation. (**B**) Responses to a 30-s pulse of pH 5.5 buffer were measured before (gray bars) and after (black bars) exposure to 750 pM NGF for 10 min. Responses from five or six oocytes per construct are normalized to maximal currents obtained with a saturating dose of capsaicin (10 μM). Potentiation is measured as the fold increase in response to a 30-s challenge with pH 5.5 buffer after 10-min treatment with 750 pM NGF: 39.0 ± 9.5 (TRPV1); 0.94 ± 0.9 (TRPV1Δ777–820); 1.24 ± 0.1 (TRPV1Δ777–792); 2.45 ± 0.3 (TRPV1Δ784–792); 3.17 ± 0.5 (TRPV1Δ784–789); 2.51 ± 0.4 (TRPV1 R785Q, K788Q); and 2.61 ± 0.5 (TRPV1 K788Q, R797Q) (*25*). (**C**) Heat-evoked currents were measured in response to temperature ramps and normalized to a saturating dose of capsaicin (10 μM). Traces are representative of responses from four or five oocytes per construct. Light blue (TRPV1); dark blue (TRPV1 R785Q, K788Q); purple (TRPV1Δ784-789); green (TRPV1 K788Q, R797Q); yellow (TRPV1 Δ784-792); orange (TRPV1Δ777–792); and red (TRPV1Δ777–820). Average responses at subthreshold and suprathreshold temperatures are plotted in (**D**). In all experiments, oocytes also expressed TrkA/p75.

The most well characterized PIP_2-binding domains in channels are those of the inward rectifier potassium (IRK) channels. All members of this family are thought to be positively regulated by PIP_2 interaction (*1*), although binding affinities differ among family members (*11*, *12*). Even though PIP2 activates IRKs and inhibits TRPV1, are regulated in opposite directions by PIP_2, we asked whether potentiation could be restored to TRPV1Δ777–820 by inserting a region from an IRK family member. Chimeras of TRPV1 were therefore generated in which amino acids 777 to 820 were replaced with residues 207 to 244 from the cytoplasmic C-terminal tail of IRK1 (Fig. 3A), a region shown to be important for PIP_2-dependent activity of this channel (*11*). The resultant chimera (TRPV1.IRK) was responsive to capsaicin, protons, and heat but showed relatively small currents compared with those of wild-type TRPV1 (29.4 ± 3.5% for pH 5.5) (*10*), even though these channels were expressed at comparable levels, as determined by cell surface biotinylation (fig. S1). This apparent decrease in activity was accompanied by a marked rightward shift in half-maximal effective concentration for capsaicin (EC_{50} = 3.0 ± 0.2 μM for chimera and 0.42 ± 0.03 μM for wild-type TRPV1, Fig. 3B), which suggests that the PIP_2-binding domain from IRK1 enhances interaction of the channel with phospholipids, and thus renders it more avidly inhibited than wild-type TRPV1.

PLC-mediated modulation of IRK1 is nearly undetectable in *Xenopus* oocytes (*13*), presumably reflecting the relatively high affinity of this channel for PIP_2, and our initial attempts to potentiate the TRPV1.IRK chimera were similarly unsuccessful. We therefore asked whether the presumed high affinity of this chimera for PIP_2 could be overcome, by either lowering phospholipid availability or weakening PIP_2 affinity. Phenylarsine oxide (PAO) is a cell-permeable, reversible inhibitor of phosphatidylinositol 4-kinase that limits PIP_2 resynthesis (*14*). Treatment of TRPV1-expressing oocytes with PAO potentiated proton-evoked currents, and subsequent activation of TrkA receptors had minimal additional effect on channel activity (Fig. 3C). To further decrease PIP_2 levels, we combined PAO treatment with activation of EGFR. Unlike TrkA, this PLC-coupled receptor can be expressed at high levels in oocytes without toxicity, which allows for reliably robust ligand-dependent cleavage of PIP_2 (*10*). Cells expressing wild-type or TRPV1.IRK channels showed significant potentiation (fold increase of 11.3 ± 2.5 and 4.0 ± 0.8, respectively) when treated with EGF and PAO for 5 min, whereas TRPV1Δ777–820 showed no potentiation (fold increase of 0.75 ± 0.02) (Fig. 3D). These results demonstrate that the PIP_2-binding domain from IRK1 can substitute for residues 777 to 820 of TRPV1 and support potentiation, so long as PIP_2 levels are sufficiently diminished.

To structurally weaken PIP_2-channel interactions, we generated a TRPV1.IRK1 chimera harboring a mutation [Arg^{218} replaced by Gln (R218Q)] that in the context of IRK1 produces a channel with faster kinetics of inhibition, which suggests a decreased affinity for PIP_2 (*11*). This chimera (TRPV1.IRK R218Q) showed significantly greater potentiation than TRPV1.IRK and was indistinguishable from wild-type TRPV1 in this regard (Fig. 3E). Fur-

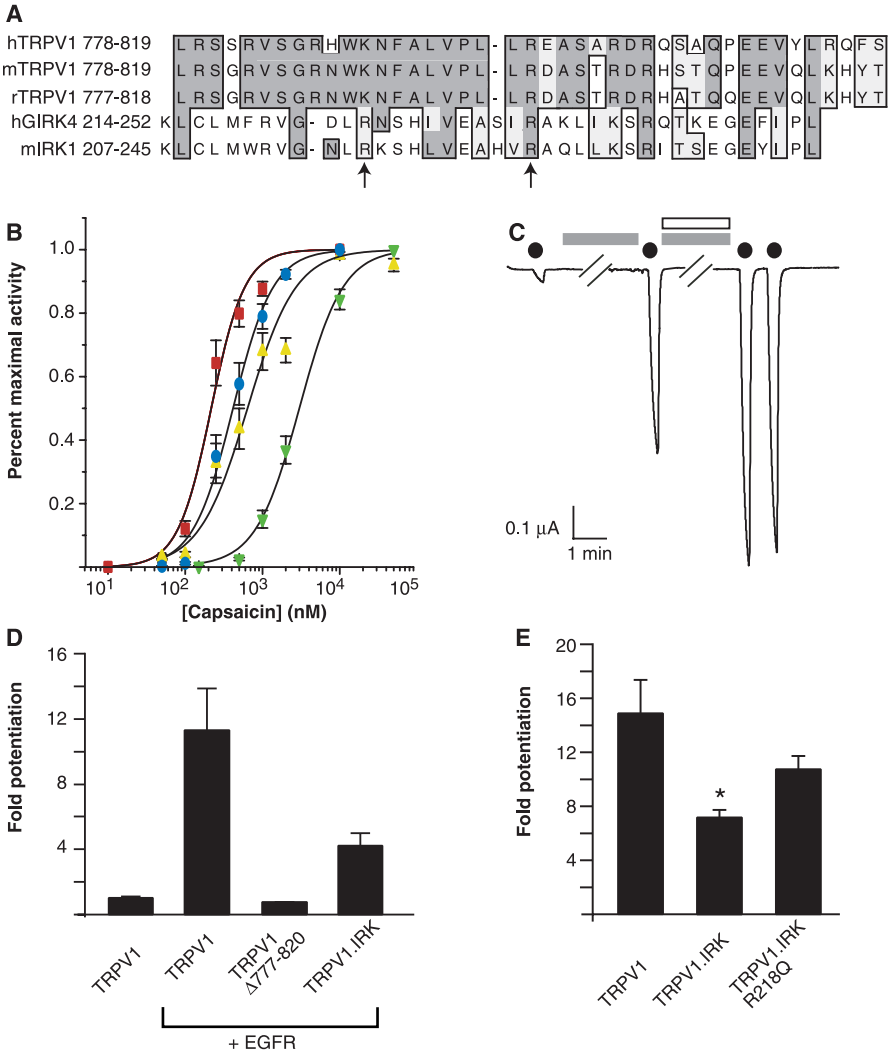

Fig. 3. Functional conservation of a PIP_2-binding domain from distinct ion channel families. (**A**) Comparison of TRPV1 C-terminal regions with putative PIP_2-binding domains from IRK1 and GIRK4 (*11*, *12*). Two basic residues required for PIP_2 interaction in IRK and GIRK are indicated with black arrowheads (●). (**B**) Agonist-response relationships for TRPV1 and mutants. Responses at each dose of capsaicin were normalized as percentage of maximal activity for each mutant. red, TRPV1Δ777–820; blue, TRPV1; yellow, TRPV1.IRK R218Q; green, TRPV1.IRK. Data were fit to the Hill equation, yielding the following hill coefficients: 1.68 ± 0.18 (TRPV1, n = 8); 2.0 ± 0.31 (TRPVΔ777–820, n = 11); 1.39 ± 0.19 (TRPV1.IRK R218Q, n = 8); 1.54 ± 0.10 (TRPV1.IRK, n = 5). (**C**) Inhibition of phosphatidylinositol 4-kinase enhances TRPV1-mediated currents. Representative voltage-clamp trace (E_{hold} = −45 mV) from a TRPV1-expressing oocyte challenged with pH 5.5 buffer (30 s; black dots). Protons elicited a small current that was greatly enhanced after 10-min exposure to PAO (30 μM, gray bars). Further treatment with NGF (750 pM, white bar) and PAO (30 μM, 10 min) produced only minimal further enhancement. (**D**) Replacement of the C-terminal basic domain of TRPV1 with the PIP_2-binding site of IRK1 yields channels that can still be potentiated. Oocytes expressing constructs indicated at bottom (along with EGFR, where indicated) were exposed to pH 5.5 buffer for 30 s before and after 5-min treatment with EGF (50 ng/ml) and PAO (15 μM). Potentiation represents the fold increase in current in five to eight oocytes per construct after treatment with EGF and PAO. (**E**) PIP_2 binding affinity correlates with ability of chimeric channels to be potentiated. Oocytes expressing wild-type or chimeric channels, together with EGFR, were exposed to pH 5.5 buffer for 30 s before and after 5-min treatment with EGF (50 ng/ml) and PAO (15 μM). Potentiation represents the fold increase in current in five oocytes per construct after treatment with EGF and PAO. Asterisk indicates $P < 0.02$ (Student's t test). No statistical difference was seen between TRPV1 and TRPV1.IRK R218Q.

thermore, the capsaicin dose-response curve for TRPV1.IRK R218Q was closer to that obtained with wild-type TRPV1 channels (Fig. 3B), consistent with a return to a milder form of PIP_2-mediated inhibition than found in TRPV1.IRK. Furthermore, consistent with their relative EC_{50} values for capsaicin, TRPV1.IRK-mediated currents were activated only at very high temperatures (48° ± 0.4°C), whereas the chimera with weakened PIP_2 binding affinity (TRPV1.IRK R218Q) had a thermal threshold (44° ± 0.3°C) closer to that of wild-type TRPV1 channels (44°C) (Fig. 4, A and B).

Several reports have recently suggested that potentiation of TRPV1 is achieved through protein kinase C (PKC)–dependent channel phosphorylation (*15*, *16*). Moreover, two putative phosphorylation sites on TRPV1 have been identified, and mutations at these residues abolish phorbol ester–mediated potentiation of capsaicin-evoked currents (*17*). One of these sites, S800, is contained within the region that we implicate in PIP_2-mediated inhibition, and we therefore asked whether phosphorylation at this site is required for receptor tyrosine kinase–mediated potentiation. Accordingly, we mutated S800 and found that this mutant (TRPV1 S800A) displayed normal capsaicin-evoked currents and normal EGFR-mediated potentiation (fold increase of 6.6 ± 1.2 for wild-type TRPV1 and 5.1 ± 0.5 for S800A, Fig. 4C). TrkA activation also produced robust potentiation of both wild-type and S800A channels, although a statistically significant difference was observed in the absolute magnitude of the effect (fold increase of 17.1 ± 6.1 for wild-type and 8.6 ± 0.5 for S800A, Fig. 4D). Thus, phosphorylation at S800 is not absolutely required for EGFR- or TrkA-mediated potentiation. Additionally, phosphorylation by PKC probably does not contribute to potentiation of the TRPV1.IRK chimeras, because the PIP_2-binding domain from IRK1 contains no PKC consensus sites, yet it supports significant receptor-mediated potentiation in the context of TRPV1. Indeed, robust potentiation can also be achieved simply by inhibition of PIP_2 synthesis, independent of either PLC or PKC activation (Fig. 3C). However, the reduced level of TrkA-mediated sensitization observed with the S800A mutant raises the possibility that phosphorylation can modulate potentiation efficacy, perhaps by increasing negative charge density at this site and weakening electrostatic interactions between PIP_2 and the channel. Alternatively, we have shown that TrkA (but not EGFR) forms a complex with TRPV1 and PLC-γ (*3*), and thus the reduced sensitization of the S800A mutant by NGF could also reflect a decreased physical interaction and efficiency of local PIP_2 hydrolysis.

Our findings provide a structural basis to support the hypothesis that PLC-mediated regulation of TRP channels involves the removal of PIP_2 from a binding site on the channel protein. Although PIP_2-binding domains in channels exhibit little linear sequence homology, our studies suggest that they function as modular regulatory domains that mediate inhibition or activation by phospholipids depending on their channel context. Several TRP channels can be directly activated in vitro by DAG or other polyunsaturated lipids, such as anandamide in the case of TRPV1 (*2*, *18*, *19*). These lipid second messengers could activate or modulate TRP channels by displacing PIP_2 from an inhibitory binding site on the channel complex. However, capsaicin and anandamide sensitivity map to a domain that is distinct from the C-terminal region identified here as being important for PLC modulation (*20*). Furthermore, TRPV1 mutants that lose the ability to be potentiated retain capsaicin sensitivity, which suggests that PIP_2 and unsaturated lipid agonists interact with TRP channels at separable sites, at least in the case of TRPV1.

The capsaicin receptor TRPV1 is normally activated with a threshold that corresponds to the onset of tissue damage and pain (~43°C) (*6*). Our studies suggest that this physiologically crucial set point is determined, at least in part, by the strength of TRPV1-PIP_2 interactions. If this interaction were too strong, then the activation threshold would be too high to serve as an effective warning mechanism, as is illustrated by the VR1.IRK chimera. The more tempered affinity of TRPV1 for PIP_2 not only establishes a physiologically relevant

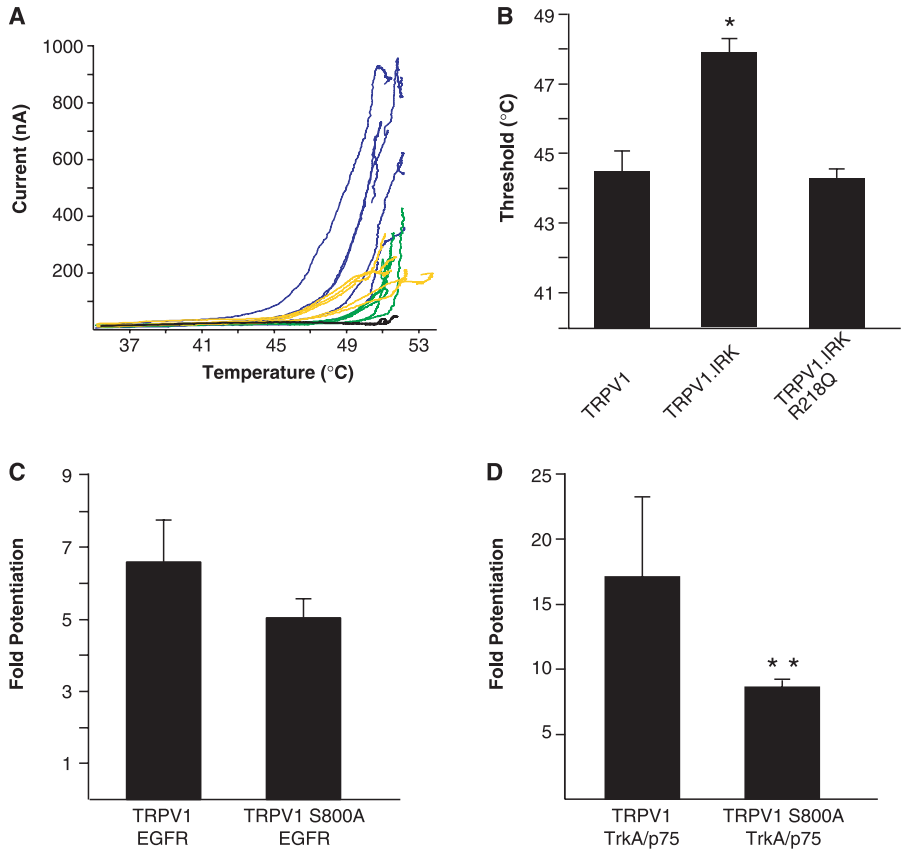

Fig. 4. PIP_2-binding affinity correlates with temperature sensitivity. (**A**) Representative temperature-response profiles from oocytes expressing TRPV1 or TRPV1.IRK chimeras. Each trace represents a single oocyte expressing TRPV1 (blue), TRPV1.IRK (green), or TRPV1.IRK R218Q (yellow). Currents obtained from water-injected oocytes are indicated in black. (**B**) The average temperature response threshold (*24*) for oocytes expressing TRPV1.IRK (47.9° ± 0.4°C) was significantly higher than for those expressing wild-type TRPV1 (44.5° ± 0.6°C, asterisk indicates $P < 0.01$, Student's *t* test, for five oocytes per construct). No significant difference was seen between TRPV1 and TRPV1.IRK R218Q (44.3° ± 0.3°C). (**C**) Mutation of a putative PKC phosphorylation site has no effect on EGFR-mediated potentiation. Oocytes expressing wild-type or S800A mutant channels, together with EGFR, were exposed to capsaicin (250 nM for 30 s) before and after treatment with EGF (100 ng/ml for 5 min). Potentiation represents the fold increase in current in eight oocytes per construct after treatment with EGF. No significant difference was seen between TRPV1 and TRPV1S800A (Student's *t* test). (**D**) Oocytes expressing wild-type or S800A mutant channels, together with TrkA/p75, were exposed to capsaicin (250 nM for 30 s) before and after treatment with NGF (750 pM for 10 min). Potentiation represents the fold increase in current after treatment with NGF (double asterisk indicates $P < 0.02$, Student's *t* test, for nine oocytes per construct).

activation threshold, but also enables the channel to be dynamically modulated by inflammatory products that activate PLC. Finally, it is interesting to note that the C-terminal domain of TRPV3, a warm-sensitive channel with an activation threshold of ~35°C (*21–23*), conspicuously lacks a region corresponding to the 777–792 domain of TRPV1, the minimal essential core of the predicted PIP_2 binding site. Thus, modification of this PIP_2 regulatory domain by genetic, biochemical, or pharmacological mechanisms may have profound effects on sensitivity of primary afferent nerve fibers to chemical and thermal stimuli under normal or pathological conditions.

References and Notes

1. D. W. Hilgemann, S. Feng, C. Nasuhoglu, *Sci. STKE* **2001**, RE19 (2001).
2. R. C. Hardie, *Annu. Rev. Physiol.* **65**, 735 (2003).
3. H. H. Chuang *et al.*, *Nature* **411**, 957 (2001).
4. M. Tominaga, M. Wada, M. Masu, *Proc. Natl. Acad. Sci. U.S.A.* **98**, 6951 (2001).
5. L. W. Runnels, L. Yue, D. E. Clapham, *Nature Cell Biol.* **4**, 329 (2002).
6. M. J. Caterina *et al.*, *Nature* **389**, 816 (1997).
7. M. Tominaga *et al.*, *Neuron* **21**, 531 (1998).
8. M. J. Caterina *et al.*, *Science* **288**, 306 (2000).
9. J. B. Davis *et al.*, *Nature* **405**, 183 (2000).
10. E. D. Prescott, D. Julius, unpublished data.
11. H. Zhang, C. He, X. Yan, T. Mirshahi, D. E. Logothetis, *Nature Cell Biol.* **1**, 183 (1999).
12. C. L. Huang, S. Feng, D. W. Hilgemann, *Nature* **391**, 803 (1998).
13. E. Kobrinsky, T. Mirshahi, H. Zhang, T. Jin, D. E. Logothetis, *Nature Cell Biol.* **2**, 507 (2000).
14. C. Wiedemann, T. Schafer, M. M. Burger, *EMBO J.* **15**, 2094 (1996).
15. V. Vellani, S. Mapplebeck, A. Moriondo, J. B. Davis, P. A. McNaughton, *J. Physiol.* (*London*) **534**, 813 (2001).
16. L. S. Premkumar, G. P. Ahern, *Nature* **408**, 985 (2000).
17. M. Numazaki, T. Tominaga, H. Toyooka, M. Tominaga, *J. Biol. Chem.* **277**, 13375 (2002).
18. P. M. Zygmunt *et al.*, *Nature* **400**, 452 (1999).
19. T. Hofmann *et al.*, *Nature* **397**, 259 (1999).
20. S. E. Jordt, D. Julius, *Cell* **108**, 421 (2002).
21. A. M. Peier *et al.*, *Science* **296**, 2046 (2002).
22. G. D. Smith *et al.*, *Nature* **418**, 186 (2002).
23. H. Xu *et al.*, *Nature* **418**, 181 (2002).
24. Materials and methods, fig. S1, and associated references are available as supporting material on *Science* Online.

25. We thank R. Nicoll and D. Minor for many helpful suggestions and encouragement throughout this project, G. Reid for help with the Peltier system, and members of our laboratory for advice. This work was supported by predoctoral fellowships from the NSF and the University of California, San Francisco, Chancellor's Fund (E.D.P.) and by the NIH (D.J.).

Supporting Online Material

www.sciencemag.org/cgi/content/full/300/5623/1284/DC1
Materials and Methods
Fig. S1
References

19 February 2003; accepted 15 April 2003

The Birth of an Alternatively Spliced Exon: 3′ Splice-Site Selection in *Alu* Exons

Galit Lev-Maor,[1]* Rotem Sorek,[1,2]* Noam Shomron,[1] Gil Ast[1]†

Alu **repetitive elements can be inserted into mature messenger RNAs via a splicing-mediated process termed exonization. To understand the molecular basis and the regulation of the process of turning intronic *Alu*s into new exons, we compiled and analyzed a data set of human exonized *Alu*s. We revealed a mechanism that governs 3′ splice-site selection in these exons during alternative splicing. On the basis of these findings, we identified mutations that activated the exonization of a silent intronic *Alu*.**

Alu elements are short (about 300 nucleotides in length), interspersed elements that amplify in primate genomes through a process of retroposition (*1–3*). These elements have reached a copy number of about 1.4 million in the human genome, composing more than 10% of it (*4*). A typical *Alu* is a dimer, built of two similar sequence elements (left and right arms) that are separated by a short A-rich linker. Most *Alu*s have a long poly-A tail of about 20 to 100 bases (*5*).

Parts of *Alu* elements, predominantly on their antisense orientation, can be inserted into mature mRNAs by way of splicing ("exonization"). Presumably, the exonization process is facilitated by sequence motifs that resemble splice sites, which are found within the *Alu* sequence (*6–9*) (see fig. S1 for a model of exonization). Because *Alu*s are found in primate genomes only, *Alu*-derived exons might contribute to some of the characteristically unique features of primates.

We have previously shown that more than 5% of human alternatively spliced exons are *Alu*-derived and that most, if not all, *Alu*-containing exons are alternatively spliced (*9*). We therefore hypothesized that mutations causing a constitutive splicing of intronic *Alu*s would cause genetic diseases, and indeed we found in the literature several instances in which a constitutive *Alu* insertion caused a genetic disorder (*10–12*).

To study the alternative splicing regulation of exonized *Alu*s, we compiled a data set of exonized *Alu*s from the human genome. An analysis of this data set revealed that two positions along the inverted *Alu* sequence are most commonly used as 3′ splice sites (3′SSs) in *Alu* exonizations: position 279 ("proximal AG") and position 275 ("distal AG"). The relationships between two near AGs in a 3′SS were well characterized previously in the context of constitutive splicing (*13*, *14*). To pinpoint the sequence determinants by which the spliceosome selects one of the two possible AGs in the context of alternative splicing, we aligned the exonized *Alu*s that use either of these AGs to their ancestor.

The 3′SS regions of these instances are shown in Fig. 1. Figure 1 also shows that the proximal AG is selected mostly in exonized *Alu*s of S subfamilies (9 times out of 13), whereas the distal AG is mainly selected in exonized *Alu*s belonging to J subfamilies (12 times out of 16). This differential usage of AG selection in *Alu* subfamilies is probably because of the polymorphism between the J and S subfamilies in position 277 (Fig. 1, colored yellow), which eliminates the distal AG in *Alu*s of the S subfamilies. As a result, the proximal AG is selected. Although another polymorphism at position 275 creates a new distal AG in the S subfamilies, this new AG is six nucleotides downstream from the proximal AG, a distance that was shown to be out of the effective range for selecting a distal AG in constitutive splicing (*14*). Indeed, the cases where *Alu*s of the S subfamilies used the distal AG required mutations that shortened the distance between AGs back to four nucleotides (Fig. 1, colored green). This indicates that when the range between the two AGs is four nucleotides or less the distal AG is preferred and when the distance is six nucleotides or more the proximal is preferred.

However, in five cases (Fig. 1, rows 25 to 29), the proximal AG was selected, even though a distal AG existed less than six nucleotides in range; in all these cases, the G in position –7 (colored purple) was mutated to either A (two cases) or T (three cases). Remarkably, a mutation in the same position in intron 5 of the COL4A3 gene leads to exonization of a silent intronic *Alu*. This *Alu* exon is constitutively spliced, resulting in an Alport syndrome phenotype (*10*). This implies that the G in position –7 suppresses the selection of the proximal AG, causing a shift toward selection of the distal AG. When this G is mutated, the proximal AG is preferred.

[1]Department of Human Genetics and Molecular Medicine, Sackler Faculty of Medicine, Tel Aviv University, Ramat Aviv 69978, Israel. [2]Compugen, 72 Pinchas Rosen Street, Tel Aviv 69512, Israel.

*These authors contributed equally to this work.
†To whom correspondence should be addressed. E-mail: gilast@post.tau.ac.il